Journal of Nuclear Science and Technology

ISSN: 0022-3131 (Print) 1881-1248 (Online) Journal homepage: https://www.tandfonline.com/loi/tnst20

Investigations of the melting behaviour of the U–Zr–Fe–O system

Paul David W. Bottomley, Mairead Murray-Farthing, Dario Manara, Thierry Wiss, Bert Cremer, Cos Boshoven, Patrick Lajarge & Vincenzo Rondinella

To cite this article: Paul David W. Bottomley, Mairead Murray-Farthing, Dario Manara, Thierry Wiss, Bert Cremer, Cos Boshoven, Patrick Lajarge & Vincenzo Rondinella (2015) Investigations of the melting behaviour of the U–Zr–Fe–O system, Journal of Nuclear Science and Technology, 52:10, 1217-1225, DOI: 10.1080/00223131.2015.1023381

To link to this article: https://doi.org/10.1080/00223131.2015.1023381

Published online: 10 Apr 2015.

Journal of Nuclear Science and Technology, 2015
Vol. 52, No. 10, 1217–1225, http://dx.doi.org/10.1080/00223131.2015.1023381

Taylor & Francis
Taylor & Francis Group

ARTICLE

Special Issue for ANFC2014

Investigations of the melting behaviour of the U–Zr–Fe–O system

Paul David W. Bottomley*, Mairead Murray-Farthing, Dario Manara, Thierry Wiss, Bert Cremer, Cos Boshoven, Patrick Lajarge and Vincenzo Rondinella

European Commission, Joint Research Centre, Institute for Transuranium Elements, Hermann-von-Helmholtz Pl. 1, Postfach 2340, 76125 Karlsruhe, Germany

(*Received 18 October 2014; accepted final version for publication 9 February 2015*)

During a severe nuclear accident, the UO_2 fuel rods, Zircaloy cladding, guide tubes, absorber and steel structural components inside the reactor pressure vessel overheat and a series of interactions between these elements and the steam atmosphere occur. These produce more heat in addition to the decay heat and result in a liquid corium of oxidic and metallic phases depending on the exact conditions and processes. A major systems resulting from this is the U–Zr–Fe–O system. High-temperature data for this system is important in order to be able to model these interactions. The Joint Research Centre, Institute for Transuranium Elements (JRC-ITU) has been examining the melting ranges for this system over the whole FeO range by means of a specialized laser flash technique that achieves very high temperatures and avoids crucible contamination. The melted zones were examined for their structure, composition and for estimation of the liquidus and solidus temperatures. The results showed that with FeO contents of over 20mol% there was a very large melting range that would permit long liquid cooling times and extend the relocation of fuel material within the reactor pressure vessel. Based on these results, the main phase regimes expected under severe accident conditions could be identified.

Keywords: severe accident; reactor safety; uranium dioxide; zirconium oxide; iron oxide; in-vessel retention; corium chemistry

1. Introduction

In order to be able to understand the important interactions that take place during the degradation of fuel and the loss of its geometry to form molten material during a severe reactor accident, then it is necessary to understand the basic ceramic systems that are found in the corium. This has been one of the aims of the MCCI (Molten Corium Concrete Interaction) work package of the European Severe Accident Research NETwork of excellence (SARNET 1 and 2); these were part of the European Commission's 5th and 6th Framework Programmes. Much research has already been done on the UO_2 and ZrO_2 systems both within the framework programmes (e.g. COLOSS and CIT) [1–8] and elsewhere [9–13] as an initial corium resulting from interactions between UO_2 fuel and steam-oxidized Zircaloy cladding. The next stage is the interaction with the reactor's internal steel structures, so that understanding of the FeO–UO_2–ZrO_2 interactions or the U–Zr–Fe–O system is the next logical step in building up knowledge of the corium properties in a systematic way. This is already more complicated as FeO is not a refractory system compared to either UO_2 or ZrO_2, and has mutually poor solubility in either UO_2 or ZrO_2 oxides. By contrast UO_2–ZrO_2 has a certain solid solubility at lower temperatures up to a complete solubility at the highest temperatures.

At The Joint Research Centre, Institute for Transuranium Elements (JRC-ITU), Karlsruhe, the contribution to the MCCI programme within SARNET was to fabricate a series of samples of the UO_2–ZrO_2–FeO system and examine the melting ranges for the whole FeO range by means of a specialized laser flash technique. Then characterize and verify their composition and determine the melting ranges (or liquidus and solidus temperatures) of the samples and quantify the main features of this systems phases and the high-temperature melting behaviour relevant to severe accidents. These data are also highly relevant to the modelling of reactor material degradation.

*Corresponding author. Email: paul.bottomley@ec.europa.eu

Table 1. Compositions of the prepared $(1-x)/2\%UO_2-(1-x)/2\%ZrO_2-x$mole%FeO samples.

Oxide	Mole%				
UO_2	45	40	30	20	10
ZrO_2	45	40	30	20	10
FeO	10	20	40	60	80
Value of x	0.1	0.2	0.4	0.6	0.8

2. Method

2.1. *Fe–U–Zr–O system samples and their preparation*

The five different compositions of the finely ground components were prepared, along with a small addition of Fe powder (3wt%) to maintain the iron oxide in the ferrous state. The components were well-mixed in a drum for 1 hour, before pressing as pellets (1 cm diameter by 5 mm height) at ca. 600 MPa. Then, they were sintered in a Mo crucible at 1200 °C for 6 hours under an Ar atmosphere, before being removed.

The compositions ranged from $x = 10$ to 80mol%FeO (or 3.9wt% to 59.4wt%FeO) in the system $(1-x)/2\%UO_2-(1-x)/2\%ZrO_2-x$mol%FeO and are given in **Table 1**.

They were then characterized to verify their composition and physical condition by X-ray diffraction (XRD) and by sectioning and examination of the cross-section by optical microscopy (OM).

2.2 *Sample preparation after laser flash pyrometry*

After the samples had been heated by laser shot pyrometry to determine the melting transitions by interpretation of the thermograms, they were then sectioned across the melted zone and one half was then mounted and grounded on successively finer silica abrasion discs and finally diamond cloths (down to 1 μm) before examination of the various phases present in the sample (particularly in the melt zone) by means of Leica optical microscope and a JOEL scanning electron microscopy with energy dispersive analysis (OM and SEM–EDX).

2.3. *JRC-ITU-fast laser flash (FLF) facility*

JRC-ITU Karlsruhe has constructed a coupled laser flash-fast pyrometry facility in a glove box that is able to use materials such as UO_2 or its mixtures (**Figure 1**). The device heats the centre of a flat ground sample (approx. 8 mm dia.) of the test material in a closed cell under 3 bar Ar (or, if needed, another gas mixture) by firing a high power laser pulse (~5 mm beam dia.). The power laser melts the sample surface by heating to approximately 2500 °C in several hundred milliseconds, and then on switching off, the sample is allowed to cool. The sample's surface temperature is measured by a high-speed two-wavelength pyrometer ($\lambda = 645$ and 488 nm) every 10 microseconds (10^{-5} s) and by a multi-channel spectrometer approximately every millisecond over ~180 wavelengths ($\lambda = 550$–910 nm). This gives the bright body temperature; the absolute emissivity (ε_0) is evaluated from the variation of spectral intensity versus wavelength on 180 spectral plots recorded by the spectrometer and so the bright body temperature values are corrected to absolute temperatures. The accuracy is generally about ±25 K at the highest temperatures. In addition, there is a low power blue light diode laser irradiating the surface and this is monitored by another charge coupled detector (CCD) detector. This records any movements of the surface (as a noisy/variable signal) and is a confirmation that a liquid phase is present on the surface. A small plateau in the temperature (thermal arrest) indicates that a phase transition is occurring; this is most evident during the cooling curve. The testing was per-

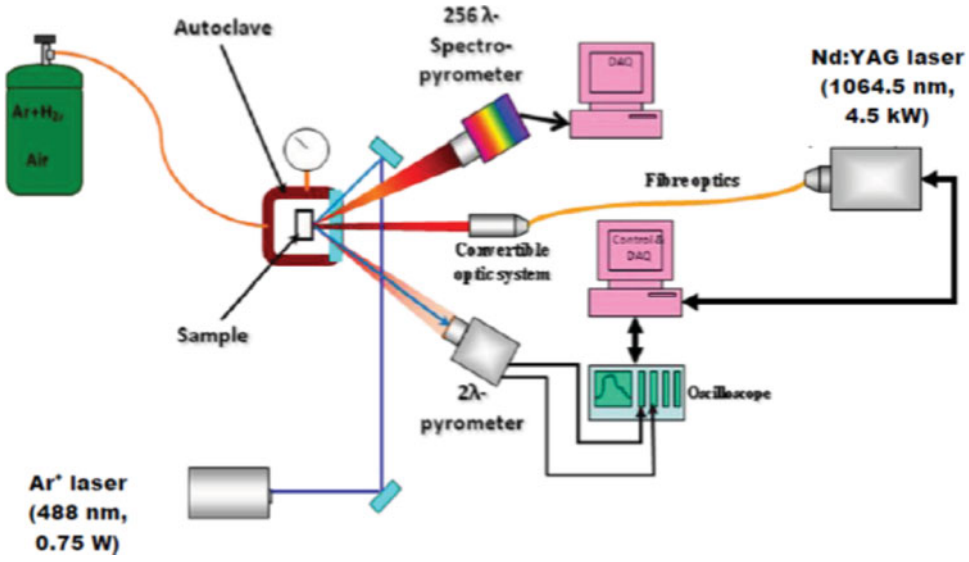

Figure 1. Fast laser flash (FLF) pyrometry facility at JRC-ITU Karlsruhe.

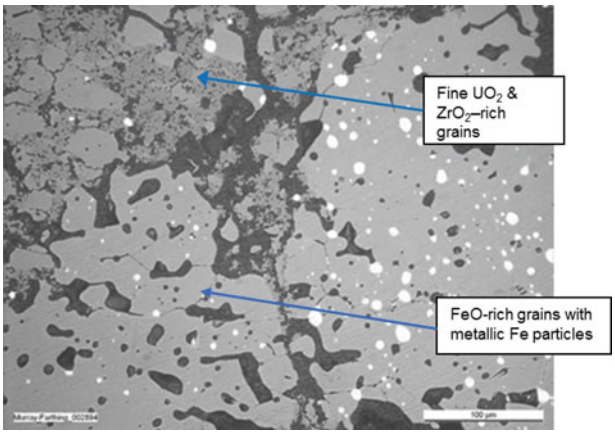

Figure 2. Micrograph of the 20%UO_2–20%ZrO_2–60%FeO (mol%) samples before testing showing large Fe-rich particles and fine-grained ZrO_2–UO_2 components (Mag. 200 ×).

formed in a glass-sided cell under pressurized inert gas (3 bar Ar) to avoid volatilization and compositional 'drift'. More details of the technique are given in references [14–16]. Post-test examinations are done on cross-sections of the sample molten zone by OM and SEM–EDX to determine the composition of the molten material along with their melting and solidification points. This helps in establishing the limits of the phase domains [17–19].

3. Results

3.1. Sample pre-'laser flash' characterization

As an example of the series of samples, the microscopic structure of the 20%UO_2–20%ZrO_2–60%FeO sample after pressing is given in **Figure 2** and shows the different FeO-rich and (Zr, U)O_2-rich phases present.

Characterization also included XRD of the pellets; the results of the XRD pattern of 20%UO_2–20%ZrO_2–60%FeO sample are shown in **Figure 3**; this confirmed the presence of three components as stoichiometric UO_2, ZrO_2 and FeO and that no oxidation has occurred during production.

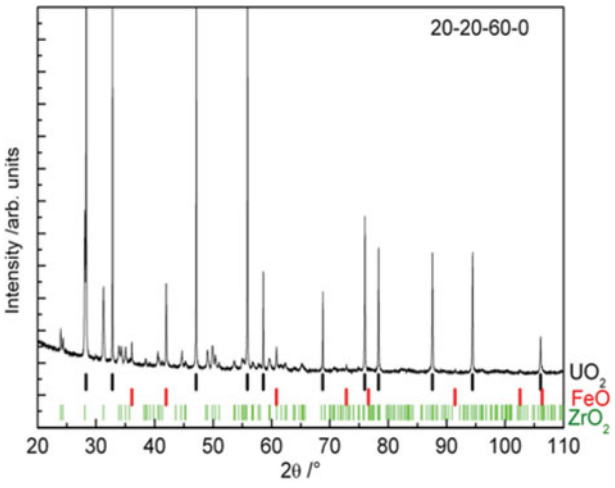

Figure 3. X-ray diffraction results of the as-fabricated sample: 20%UO_2–20%ZrO_2–60%FeO (molar ratio).

3.2. Laser flash pyrometry results

3.2.1. Laser shots of high (80mol% and 60mol%) FeO melts

In the laser shots of the high Fe-content melts, the FeO final freezing is very clearly and reproducibly seen. However higher temperature freezing also appears and it is clearly due to the solidification of the refractory components ZrO_2 and UO_2. The thermal arrests are noted as follows:

For 10%UO_2–10%ZrO_2–80mol%FeO (**Figure 4**), a thermal arrest was observed at 2500 K which was attributed to a (U,Zr)O_2 liquidus point transition; a second high-temperature arrest at 1960 K was attributed to a (U,Zr)O_2 solidus transition. The final low-temperature arrest was observed at 1624 K due to the FeO freezing. For 20%UO_2–20%ZrO_2–60mol%FeO composition, there was an arrest at 2713 K attributable to a (U,Zr)O_2 liquidus point; a second high-temperature thermal arrest at 2040 K was attributed to a (U,Zr)O_2 solidus point. Finally, there was a large inflection at 1600 K, attributable to the freezing of the dominant FeO phase.

3.2.2. Laser shots of medium (40mol%) FeO melt

The laser shots of the 30%UO_2–30%ZrO_2–40%FeO show three different arrests in temperature that correspond to a change in phase (see **Figure 5**). The interpretation of the thermal arrests of the 30%UO_2–30%ZrO_2–40mol%FeO melt composition are as follows: (1) the arrest at 2757 K is attributed to the (U,Zr)O_2 liquidus transition; (2) the thermal arrest at 2270 K is attributed to a (U,Zr)O_2 solidus transition. Again a final low-temperature arrest is observed at 1600 K attributed to the FeO-rich phase freezing.

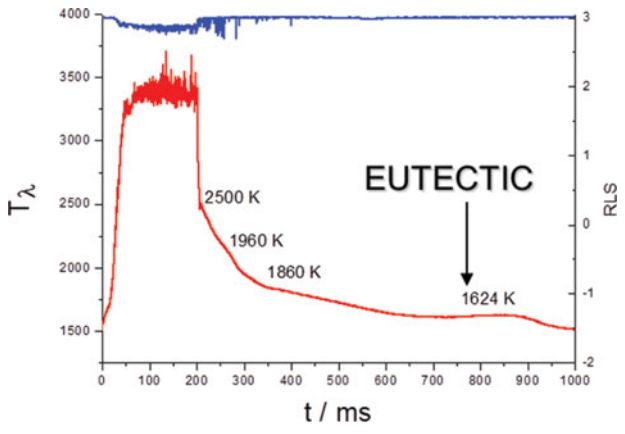

Figure 4. Thermogram of 10%UO_2–10%ZrO_2–80mol%-FeO.

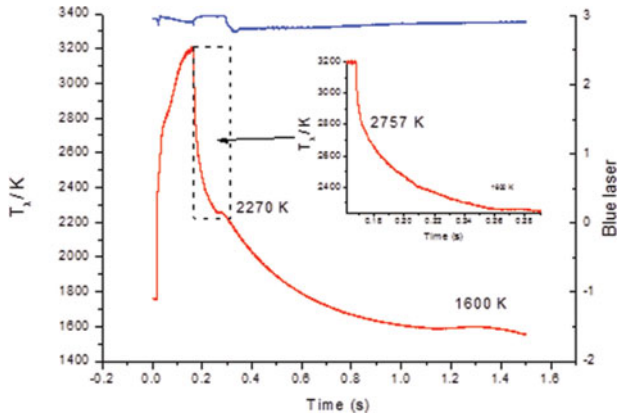

Figure 5. 30%UO_2–30%ZrO_2-40mol%FeO: 3rd laser shot with expansion to show details of cooling thermogram.

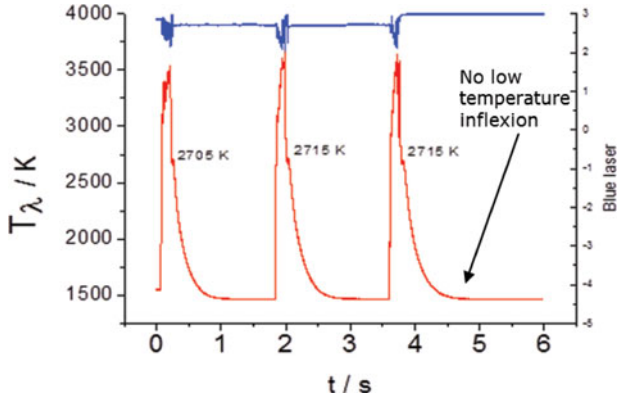

Figure 6. Laser shots of 45%UO_2–45%ZrO_2–10mol%FeO sample.

3.2.3. *Laser shots of low (20mol% and 10mol%) FeO melts*

For the 40%UO_2–40%ZrO_2–20mol%FeO sample, very little low-temperature eutectic in the freezing curve was observed, by contrast in the 10mol% FeO melt (see **Figure 6**) there is no lower eutectic melt in the freezing curve (see arrow indicating expected position).

Again the high-temperature thermal arrests can be linked to the elevated refractory UO_2–ZrO_2 content. The higher temperature arrests for the 40%UO_2–40%ZrO_2–20mol%FeO, were at 2570 K that is attributable to a (U,Zr)O_2 liquidus point; there was a second arrest at 2530 K that could be a (U,Zr)O_2 solidus point. The slight, final low-temperature arrest at 1620 K is attributable to FeO freezing. The high-temperature arrest(s) in the 20% FeO melt were slightly below from that expected from the composition.

For the 45%UO_2–45% ZrO_2–10mol%FeO (**Figure 6**), there was a thermal arrest at 2715 K attributable to a (U,Zr)O_2 liquidus transition (in previous shots arrests at 3010 and 2700 K had been observed). No second high-temperature arrest was observed that could have been attributed to the (U,Zr)O_2 solidus point (in a previous shot a transition at 2400 K had been noted). This suggests that the second shot

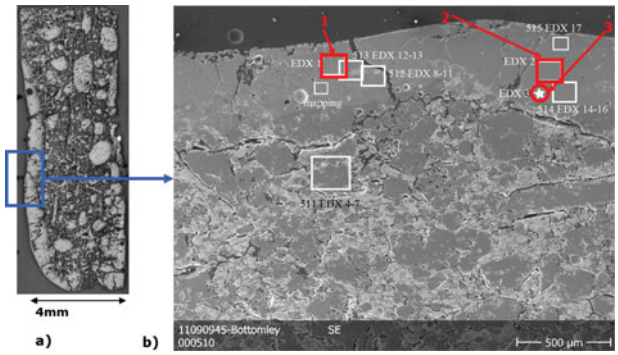

Figure 7. (a) Optical macroscope and (b) SEM micrograph of the 10%ZrO_2–10%UO_2–80mol%FeO sample.

(illustrated above) showed little segregation of the phases while some segregation had occurred in first shot. By contrast with the 20mol% FeO melt there was no low-temperature arrest (see arrow indicating expected position) due to the freezing of the FeO-rich phase in the 10mol% FeO sample. It was also absent in the previous shots.

This indicates that the level of FeO in the melt is too low to separate out as a separate phase in cooling and that this composition is dominated by the high-temperature UO_2–ZrO_2 components.

3.3. *Optical microscopy (OM) and scanning electron microscopy and analysis (SEM–EDX) results*

3.3.1. *Optical microscopy and SEM–EDX results of high (80mol%) FeO content samples*

The 80mol% FeO sample is shown in Figure 7. The melted zone is quite extensive after a number of laser shots and is up to 5 mm thick in parts. Typical for most samples the melt zone depths were of approximately 200–300 µm.

The macrograph is seen in Figure 7(a) while Figure 7(b) shows the dense melt zone on the surface. Two areas analyses at the surface and the middle with a point analysis zone at the base are given in **Table 2** and show the variation in the composition with depth. However, the averaged analysis 6.9%U–6.6%Zr and 86.5%Fe is close to the overall composition of 10%UO_2–10%ZrO_2 –80mol%FeO.

Table 2. EDX analyses in the melt zone of Figure 7(b) – area zones 1, 2 and point analysis 3 marked in red.

Analysis point	1	2	3	Average
Atom %				
Fe (Kα)	81.36	89.41	88.8	86.5
Zr (Lα)	9.13	5.09	5.54	6.6
U (Mα)	9.51	5.5	5.66	6.9

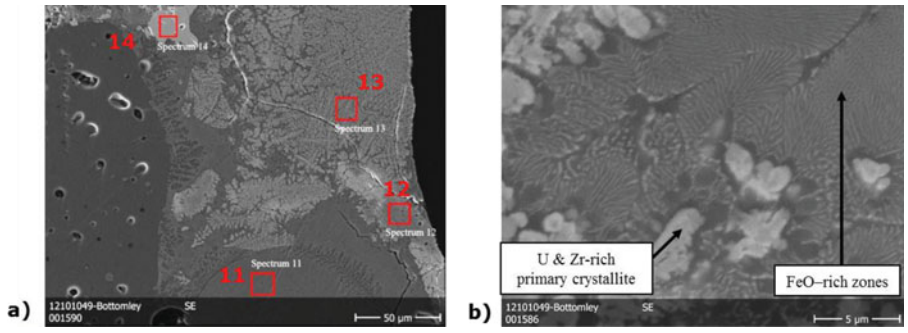

Figure 8. (a) Back-scattered image of the edge of melt zone of the 20mol%ZrO_2–20mol%UO_2–60mol%FeO sample and (b) high magnification (4000 ×) of the two-phase lamellar structure of the melt around the U, Zr-rich crystallites; the melt was Fe-rich compared to the overall composition.

The oxygen results were not consistent, therefore only the U, Zr and Fe atomic ratios were used. The Fe content varied from 81.4 to 88.8at.% Fe, while the Zr and U contents were very similar and varied between 5.5 and 9.5at.%.

The 20mol%ZrO_2–20mol%UO_2–60mol%FeO sample had three laser shots. **Figure 8(a)** shows the melt zone, which has secondary phases; the central phase is 69.4at.% FeO and 15.3 at.% of UO_2 and ZrO_2 (Spect. 13 in **Table 3**) and had an overall composition close to the initial composition. Figure 8(b) is a close-up of the melt phase surrounding the primary U, Zr crystallites; the melt phase is a fine, two-phase lamellar structure of U, Zr-richer (white) and Fe-richer (darker) phases of approximately 90at.% Fe with 5at.% of Zr and U. The lamellae are very fine with a width of 0.1–0.2 µm. The other zones were of variable composition (e.g. a UO_2-rich zone (Spect. 14) and a pure Fe particle (Spect. 11)).

3.3.2. *Optical and SEM microscopy results of medium (40mol%) FeO content sample*

Figure 9 shows a 30%UO_2–30%ZrO_2–40mol%FeO sample after testing. A dense, uniform melt zone is observed at low magnification along with the small amount of metallic iron precipitates at the edge of the melt zone but at higher magnification secondary phases are seen. In **Table 4**, the local EDS analyses are made at different depths of the molten zone. The average analysis is 31.1at.% U, 27.4at.% Zr and 41.50at.% Fe. This is not far from the original overall composition of (when oxygen content is disregarded). However, it is seen that the local compositions (Spectra 7, 8 and 9) show an enrichment in FeO at the surface (Spect. 7: ~50at.% Fe) compared to the overall composition, while the deeper composition shows a depletion in iron (Spect. 9: ~35at.% Fe). This shows that despite the rapid cooling rates a small separation of the melt still occurs. The highest FeO content at the surface corresponds to the lowest freezing composition.

Table 3. Area EDS analyses of various phases in the melt zone of Figure 8(a). The main zone (Spect. 13) shows a composition that is very close to the overall composition.

Analysis point	11	12	13	14	Average
Atom %					
Fe (Kα)	98.83	22.6	69.42	3.93	48.7
Zr (Lα)	0.91	63.31	15.25	10.3	22.44
U (Mα)	0.25	14.09	15.33	85.77	28.86

Table 4. Area EDS analyses at three different depths of the two-phase melt zone in Figure 9.

Analysis point	7	8	9	Average
Atom %				
Fe (Kα)	49.25	40.27	34.99	41.5
Zr (Lα)	22.87	28.73	30.55	27.38
U (Mα)	27.88	31	34.45	31.11

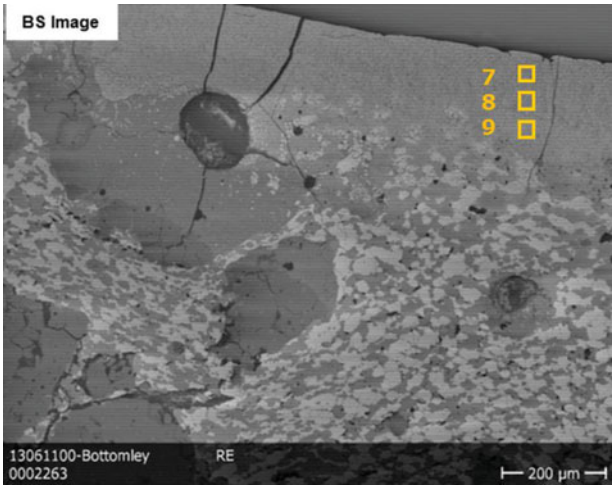

Figure 9. Back-scattered electron micrograph of the 30%UO_2–30%ZrO_2–40mol%FeO sample showing the molten zone at the sample surface. A two-phase melt structure is visible.

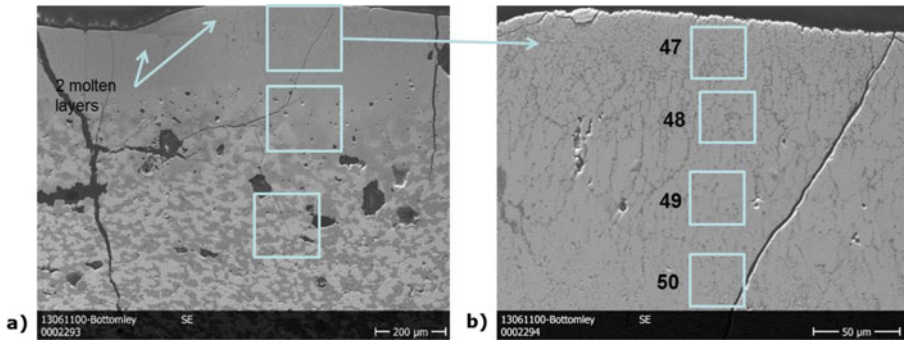

Figure 10. (a) Macrograph of a 40%UO_2–40%ZrO_2–20mol%FeO sample and (b) micrograph showing surface melt zone with major and grain boundary phases: the grain boundary phase is expected to be Fe-rich.

Table 5. EDS analyses of the melt zones with increasing depth from the surface in Figure 10(b).

Analysis point	47	48	49	50	Average
Atom %					
Fe (Kα)	29.6	24	21.62	16.35	22.89
Zr (Lα)	32.47	35.11	30.55	35.48	33.4
U (Mα)	37.44	40.89	34.45	48.17	40.24

3.3.3. Optical and SEM–EDX results of a low (10 and 20mol%) FeO content sample

Macro and micrographs of the melt zone of the 40%UO_2–40%ZrO_2–20mol%FeO sample are shown in **Figure 10(a)** and 10(b) along with the analyses in **Table 5**. The mean composition of the four points is 40.2%U–34.9%Zr–22.9at.% Fe. This corresponds reasonably well to the initial composition. Nevertheless, the analyses show a variation in the FeO content in the melt zone, with the highest concentration (i.e. lowest melting) 49.5% Fe at the surface and 35.0% Fe at the deepest melt zone. This again indicates that segregation occurs during the freezing of the melt, although the overall composition is close to the initial composition. This is also a good indication that there is no significant drift of the melt composition during the various laser shots.

It is also noted that although the Zr and U contents are close they are not identical with the Zr at.% figures always being less than the U at.% values by ~10%. The differences are just significant given the standard deviations on the Zr, U individual values. The fact that the Zr values are always higher than the U at.% values points rather to a systematic error in the quantitative analysis or curve deconvolution of the spectra.

In **Figure 11**, we can see the macro and micrographs of the 45%UO_2–45%ZrO_2–10mol%FeO sample. The analyses in **Table 6** show an average composition of 45.0%U–42.9%Zr–12.1at.% Fe. However, the FeO content varied from only 7.3at.% Fe at the bottom of the melted zone (Spect. 16) to 16.4at.% Fe at the surface (Spect. 14). The surface composition would have been the highest and final freezing point. The melt was also heterogeneous with many U-rich or Zr-rich inclusions.

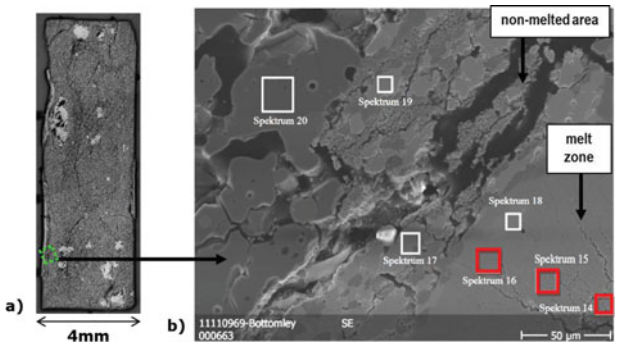

Figure 11. SEM images of the 45%UO_2–45%ZrO_2–10mol%FeO sample after testing. (a) Macroscopic cross-section of melt zone and (b) micrograph of melt zone showing a two-phase melt structure.

4. Discussion

The average value of the melt zones analyses for each sample is given in **Table 7**. This shows that the average melt zone composition for each sample corresponds closely to the overall composition. The standard deviation is also shown and this is about 7% to 3% relative (to the value) for the highest U and Zr contents (10mol% FeO) to 27% relative at the lowest Zr, U contents. For FeO, the highest relative deviation values are, as expected, highest for the lowest FeO composition (10mol% FeO) at 38% relative and fall to about 4% relative in the highest FeO composition (80% FeO). Thus, the relative deviations are similar and suggest a consistent analysis of all the three elements.

The laser flash melting shows the clear distinction in freezing behaviour of UO_2–ZrO_2–FeO system. There

Table 6. EDS analyses of three areas of melt zone marked in red in Figure 11(b) at different depths.

Analysis point	14	15	16	Average
Atom %				
Fe (Kα)	16.39	12.72	7.26	12.12
Zr (Lα)	39.79	42.81	46.19	42.93
U (Mα)	43.82	44.47	46.55	44.95

Table 7. Average analyses (and standard deviations: sd) of the molten areas of all samples.

Composition atomic%	10mol% FeO		20mol%FeO		40mol%FeO		60mol%FeO		80mol%FeO	
	av. analysis	sd.	av. analysis	sd	av. analysis	sd	av. analysis	sd	av. analysis	sd
Fe (Ka)	12.1	4.59	22.89	5.5	41.5	7.21	61.9	8.93	86.5	3.66
Zr (La)	42.95	3.2	34.86	1.3	27.38	4.01	21.1	5.65	6.6	1.81
U (Ma)	44.95	1.43	42.25	4.48	31.11	3.29	17.1	3.85	6.9	1.85
U/Zr	1.05		1.21		1.14		0.81		1.05	

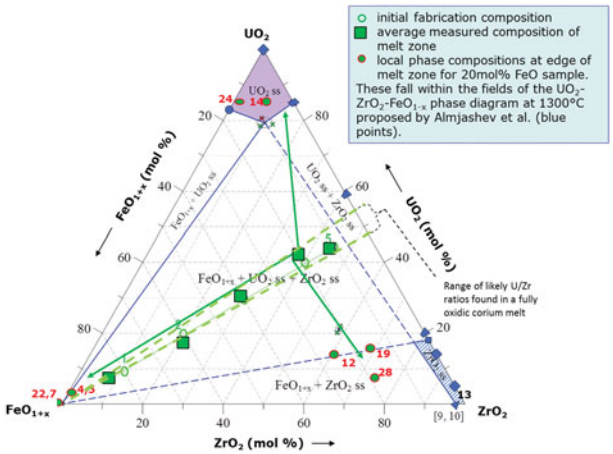

Figure 12. Pseudo-ternary diagram of the UO_2–ZrO_2–FeO_{1-x} for 1300 °C [20] showing the 5 JRC-ITU sample compositions used for the melting behaviour studies by laser flash pyrometry.

are freezing transitions between 2500 °C and 1627 °C (2757 and ~1900 K, respectively – see Figures 4 and 5) assigned to the high-melting UO_2–ZrO_2-rich phases and final transitions at 1367 °C–1327 °C (1640–1600 K) assigned to the low-melting FeO. These generally lead to an extended freezing range from 2500 °C to ~1350 °C, except for the lowest FeO content (10mol%), where only the high-melting component behaviour is evident. Calculations by Barrachin in Bakardjieva et al. [19], indicate that FeO freezing transition should still occur or be visible at 10mol% FeO in this system. These experimental results suggest that in severe accident models, this system's behaviour can be simplified by assuming a purely high-temperature behaviour at compositions below ca. 15mol% FeO content in a UO_2–ZrO_2 corium formed from degraded UO_2 fuel and oxidized Zircaloy cladding.

The SEM data from Table 7 has been has added to the UO_2–ZrO_2–FeO phase diagram at 1300 °C (by Almjashev et al. [20]) in **Figure 12**. This shows that the initial compositions and melt compositions are consistent and that therefore the melting ranges measured by the laser flash technique correspond to the initial compositions.

In addition, data from the 20mol% FeO sample (as an example) is plotted from the zones surrounding the melts that have cooled more slowly and separated into several phases. These analyses correspond very well to the various phase fields in this diagram. This is not so surprising since the final transitions in this system (solidification of FeO-rich compositions) seen in the laser flash results occur at 1330 to 1360 °C.

More importantly it indicates that the UO_2–ZrO_2–FeO phase diagram at 1300 °C (by Almjashev et al. [20]) and the melting ranges given by this work would be valid to predict an in-vessel melt's solidification behaviour in severe accident codes.

Figure 12 also illustrates that the sample compositions span the central three-component solid solution field of the system. UO_2 and ZrO_2 were held in equal molar ratios because it was expected that the melted material would contain similar quantities of both fuel and cladding.

In the Three Mile Island unit 2 (TMI-2) reactor it was estimated that the inventory of UO_2 fuel was 94,000 Kg and that of Zircaloy-4 cladding was 24,000 Kg, this corresponds approximately to the molar ratio UO_2/Zr of 0.67 [21]. Simple calculations of a cladded un-irradiated pressurised water reactor (PWR) fuel cross-section give a similar ratio of 0.66. This would suggest that the zirconium is in excess. However, the elemental U/Zr ratios of real irradiated corium samples from and above the central pool analysed in the degraded FPT0, 1 and 2 bundles of the Phébus PF project [22– 28] as well as in the TMI-2 samples [29] for a solidified fully oxidized corium are notably higher. These values ranged between 1.0 and 1.18 and are shown in Figure 12. The U/Zr values given for the melt zones in Table 7 are also close to unity (only one is below 1.0) and are in agreement with values found in real coria analysed in Phébus PF and TMI-2 investigations. Thus, this research confirms that the central equimolar zone of the UO_2–ZrO_2–FeO phase diagrams is one of the main regions of interest for in-vessel corium studies rather than the UO_2-rich ratio calculated from the reactor inventory.

5. Conclusions

(1) The UO_2–ZrO_2–FeO ternary oxide system has been investigated for its high-temperature melting and freezing behaviour.

This research shows that it can be considered as a pseudo-binary system of a high-temperature UO_2–ZrO_2

system and low-melting FeO system. This information can be used to draw a pseudo-ternary oxide phase diagram for this system.

(2) The FeO freezing transition is not observed at the lowest FeO content of 10mol% FeO, and it is estimated that the lower FeO limit for the FeO freezing tie-line in a phase diagram at ~1640 K is ~15mol% FeO.

This low-temperature behaviour is proportional to the FeO content, just as the high-temperature transitions are proportional to the combined ZrO_2–UO_2 content.

(3) At the high and medium ZrO_2–UO_2 contents one (or sometimes more) high-temperature transition(s) in the range 2500 °C –1630 °C is observed. These relate to a limited segregation of UO_2 and ZrO_2 phases, despite the rapid cooling rates.
(4) This data illustrate how the relocation of a corium is extended by the Fe oxide content and will help model the freezing behaviour of in-vessel corium.
(5) The data from the melt and nearly melted zones indicates that the UO_2–ZrO_2–FeO phase diagram at 1300 °C (Almjashev et al. [20]) can give good estimates of the expected compositions for the final solidified in-vessel corium as 1300 °C is close to the final freezing point of FeO.
(6) A roughly U, Zr-equimolar zone in the UO_2–ZrO_2–FeO diagram has been identified as the area most representative of an in-vessel corium developing in a nuclear reactor during a severe accident.

Acknowledgements

This work was carried out as part of the MCCI (Molten Corium Concrete Interaction) work package of the European Severe Accident Research NETwork of excellence (SARNET 1 & 2) that was supported by the European Commission's 5th and 6th Framework Programmes [contract number FI60-CT-2004-509065], [arrangement number 231747], respectively .

References

[1] Stuckert J, Miassoedov A, Hayward PJ, Hofmann P, Veshchunov M. ZrO_2 and UO_2 dissolution by molten zircaloy. Paper presented at: International Conference Nuclear Energy for New Europe. 2002 Sept 9–12; Kranjska Gora, Slovenia.
[2] Veshchunov MS, Stuckert J, Berdyshev AV. Modelling of Zr–O and U–Zr–O melts oxidation and new crucible tests. Karlsruhe (Germany): FZK; 2002. (Report No. FZKA 6792; SAMCOLOSS-P040 (2002)).
[3] Bottomley PDW, Barrachin M. Irradiated UO_2 fuel dissolution by liquid zircaloy: some results from the SCA Corium interactions thermochemistry project. Paper presented at: Severe Accident Research in Japan '99 (SARJ '99). 1999 Nov 8–10; Tokyo, Japan.
[4] Hofmann P, Stuckert J. ZrO_2 and UO_2 dissolution by molten zircaloy. CIT project FI4S-CT96-0032 presented at: Corium Interactions & Thermochemistry Project Meeting. 1999 Jun 7–8; Prague, Czech Republic.
[5] Hayward PJ, Hofmann P, Stuckert J, Veshchunov MS, Berdyshev AV. UO_2 dissolution by molten zircaloy. New experimental results and modelling. Karlsruhe (Germany): FZK; 1999. (Report FZKA 6379; INV-CIT(99)-P029).
[6] Müller K, Goryachev AV, Smirnov VP, Svyatkin AM, Stuckert J, Veshchunov MS, Berdyshev AV. Simultaneous dissolution of UO_2 and ZrO_2 by molten zircaloy. New experiments and modelling. Karlsruhe (Germany): FZK; 2004. (Report FZKA 6947, SAM-COLOSS-P074).
[7] Veshchunov M S, Stuckert J, Berdyshev AV. Modelling of Zr-O and U-Zr-O melts oxidation and new crucible tests. Karlsruhe (Germany): FZK; 2002. (Report FZKA 6792; SAM-COLOSS-P040).
[8] Glatz JP, Bottomley PWD, Knoche D, Papaioannou D, Romero Th, Scheindlin M. Interaction tests of molten zircaloy and irradiated fuel. Presented at: Final Meeting of the SCA COLOSS project. 2003 Jan 20–24; SCK/CEN, Mol, Belgium. (SAM-COLOSS-P0402003).
[9] Hayward PJ, George IM. Dissolution of UO_2 in molten zircaloy-4 part 1 solubility from 2000 to 2200 °C & part 2: phase evolution during dissolution and cooling. J Nucl Mater. 1994;208:35–43.
[10] Hayward PJ, George IM. Dissolution of UO_2 in molten zircaloy-4 part 3: solubility from 2000 to 2500°C & part 4: phase evolution during dissolution and cooling of 2000 to 2500 °C specimens. J Nucl Mater. 1996;232:1–13.
[11] Olander DR. Interpretation of laboratory crucible experiments on UO_2 dissolution by liquid zirconium. J Nucl Mater. 1995;224:254–265.
[12] Kim KT, Olander DR. Dissolution of uranium dioxide by molten zircaloy: I. Diffusion-controlled reaction, II. Convection-controlled reaction, J Nucl Mater. 1988;154(1):85–102.
[13] Hofmann P. Current knowledge on core degradation phenomena, a review. J Nucl Mater. 1999;270:194–211.
[14] Sheindlin M, Heinz W, Bottomley D, Knoche D, Cremer B, Somers J. Melting point measurements of the Zr-U-O system and their application. Conference presentation at: 11th Symposium on Thermodynamics of Nuclear Materials (11 STNM); 2004 Sep 6–9; Karlsruhe.
[15] Ronchi C, Sheindlin M. Melting point of MgO. J Appl Phys. 2001;90:3325. Available from: http://dx.doi.org/10.1063/1.1398069
[16] Manara D, Ronchi C, Sheindlin M, Lewis M, Brykin M. Melting of stoichiometric and hyperstoichiometric uranium dioxide. J Nucl Mater. 2005;342:148–163.
[17] Bottomley PDW, Wiss Th, Janssen A, Cremer B, Thiele H, Manara D, Sheindlin M, Murray-Farthing M, Lajarge P, Menna M, Bouexière D, Rondinella VV. Characterisation of high temperature refractory ceramics for nuclear applications. IOP Conf Ser Mater Sci Eng. 2012;32:012003. doi:10.1088/1757-899X/32/1/012003.
[18] Bottomley D, Papaioannou D, Pellottiero D, Knoche D, Rondinella VV. Investigation of high temperature irradiated fuel-liquefied zircaloy interactions in support of severe accident safety studies. IOP Conf Ser Mater Sci Eng. 2010;7:012006. doi:10.1088/1757-899X/7/1/012006.
[19] Bakardjieva S, Barrachin M, Bechta S, Bezdicka P, Bottomley D, Brissonneau L, Cheynet B, Dugne O, Fischer E, Fischer M, Gusarov V, Journeau C, Khabensky V, Kiselova M, Manara D, Piluso P,

Sheindlin M, Tyrpekl V, Wiss T. Quality improvements of thermodynamic data applied to corium interactions for severe accident modelling in SARNET2. Ann Nucl Energy. 2014;74:110–124. Available from: http://dx.doi.org/10.1016/j.anucene.2014.06.023

[20] Almjashev VI, Barrachin M, Bechta SV, Bottomley D, Defoort F, Fischer M, Gusarov VV, Hellmann S, Khabensky VB, Krushinov EV, Lopukh DB, Mezentseva LP, Miassoedov A, Petrov YuB, Vitol SA. Phase equilibria in the FeO_{1+x}–UO_2–ZrO_2 system. J Nucl Mater. 2010;400:119–126.

[21] Akers DW, Mccardell R, Russell ML, Worku G.TMI-2 core materials and fission product inventory. Nucl Energy Design. 1990;118(3):451–461.

[22] Bottomley PDW, Stalios AD, Glatz J-P, Sätmark B, Walker CT. Examination of melted fuel rods and released core material from the first Phebus FP reactor accident experiment. J Nucl Mater. 2000;278:136–148

[23] Bottomley PDW, Montigny F, Stalios A, Walker CT. EMPA of melted fuel rods from the Phebus FP reactor accident experiment. Mikrochem Acta. 1998;15:191–200.

[24] Bottomley PDW, Bremier S, Glatz J-P, Walker CT. X-ray microprobe analysis of melted fuel rods irradiated to a mean burn-up of 23 GWd/tU. Mikrochim Acta. 2000;132:391–400.

[25] Bottomley PDW, Brémier S, Papaioannou D, Walker CT. Microprobe analysis and x-ray diffraction analysis of a degraded fuel bundle: Phebus FPT1. Mikrochimica Acta. 2002;139:27–38

[26] Bottomley PDW, Bremier S, Walker CT, Glatz J-P, Papaioannou D, Arnoult J-L, Baudot D, Chareau J-M, Romero T, Schlutig S, Barrachin M, De Bremaecker A. Preliminary results of the EMPA analysis on Phebus FPT2 bundle. Paper presented at: 9th European Workshop on the Modern Developments and Applications in Microbeam Analysis (EMAS 2005). 2005 May 22–26; Florence, Italy.

[27] Bottomley D, Schlutig S, Brémier S, Barrachin M, De Bremaecker A, Walker CT, Glatz J-P, Papaioannou D, Arnoult J-L, Baudot D, Romero Th, Simondi-Teissière B. Post irradiation examination of the lower part of the Phebus FPT2 degraded bundle (Paper 7333). Paper presented at: International Congress on Advanced Power Plants (ICAPP 2007). 2007 May 13–18; Nice, France.

[28] Barrachin M, Gavillet D, Dubourg R, Debremaecker A. Fuel and fission product behaviour in early phases of a severe accident, part I: experimental results of the PHEBUS FPT2 test. J Nucl Mater. 2014;453(1–3):340–354.

[29] Bottomley PDW, Coquerelle M. Metallurgical examination of bore samples from the three mile island unit 2 reactor core. Nucl Technol. 1989;87:120–136.